Publications of the Astronomical Society of the Pacific, 129:074501 (11pp), 2017 July https://doi.org/10.1088/1538-3873/aa6f53

A Model-free CAF Fringe Search Algorithm with Wavelet Boosting for VLBI Observation

Tianyi Zhang[1], Qiao Meng[1,4], Congyan Chen[2], Weimin Zheng[3], Wei Liu[1], Quantao Yu[1], and Li Tong[3]
[1] Institution of RF-&OE-ICs, Southeast University, Nanjing 210096, China
[2] School of Automation, Southeast University, Nanjing 210096, China
[3] Shanghai Astronomical Observatory, Chinese Academy of Sciences, Shanghai 200030, China
Received 2017 January 8; accepted 2017 April 25; published 2017 May 23

Abstract

Very-Long-Baseline interferometry (VLBI) is a powerful tool in radio astronomy, geodesy, and deep space exploration. Priori predicted delay models are needed to make interferometry fringes, but in some cases they would be difficult to get. This paper proposes an effective algorithm named CAF-W algorithm to search fringes from the raw data in a large search range without priori predicted delay models. The cross-ambiguity function (CAF) is used to make a time-frequency correlation in the delay–delay rate plane. The wavelet boosting algorithm is used to eliminate interference and enhance the CAF peak, whose position would give the delay and delay rate estimations. Incoherent averaging and sliding search window techniques are used to overcome the wide search range and the poor signal-to-noise ratio in VLBI observations. The CAF-W algorithm could be performed with fast algorithms so the computation burden is affordable. This algorithm has successfully achieved VLBI fringes from the raw data without priori predicted delay models in VLBI observations.

Key words: instrumentation: interferometers – techniques: interferometric – techniques: radar astronomy

Online material: color figures

1. Introduction

Very Long Baseline Interferometry (VLBI) has become a significant technique in astronomy, geodesy and deep space exploration due to its extremely high angular resolution (Counselman 1973). Radio signals emitted by cosmic or artificial radio sources are received by multiple telescopes simultaneously. At each telescope, the signal is received by the antenna and down converted to baseband, then the digital back-ends (DBE) sample the analog signals and pack the raw data with essential information. Packed data is fed to the specific data processors called correlators to form the interferometry fringes, which will give the propagation time delay measurements between telescopes with very high accuracy (Marcello & Spencer 1989).

Due to the relative motions between sources and telescopes, the time-variant terms in the time delay cannot be ignored during the correlation processing. If the integration time in the correlation is too long, the interferometry fringe would be blurred. However, the low signal-to-noise ratio in VLBI observations requires long integration time (Clark et al. 1985). Therefore, the time-variant terms in the time delay are removed by the "fringe rotation" (also called "fringe stopping") by using the priori predicted delay models (Romney 1995).

The priori predicted delay models with enough accuracy are very important for successful VLBI correlation. However, there are some situations where the priori predicted delay models are not precise enough. The model errors may be caused by errors in the source or antenna position used, errors in the Earth model, errors in clock drift and errors in atmospheric models (Cotton 1995). In some worse cases, the priori predicted delay models would even be unavailable.

In order to reduce the priori predicted delay model errors, fringe fitting techniques are used to estimate the residuals between the priori predicted delay models and real observations, then the priori predicted delay models are revised with these residuals. A widely used technique, named FFT (fast Fourier transform) fringe search algorithm, could fit a single baseline each time (Cotton 1995; Nakajima et al. 2001; Petrov et al. 2007). The fringe rotation is first performed using the inaccuracy priori predicted delay model, then the time series of the cross-spectrum are calculated and Fourier transformed to the delay–delay rate domain. The residuals of the delay and delay rate can be obtained by locating the maximum amplitude in this two-dimensional (2D) plane (Moran 1976).

The search resolution of FFT fringe search algorithm is quite high while its search range is desired to be as narrow as possible in order to reduce the probability of false detection (Cotton 1995). However, in some situations, e.g., the first observation with new instruments or at new telescopes, errors in the priori predicted delay models would be too large for the FFT fringe search algorithm to fit. In these cases the correlation

[4] Corresponding author.

processing is almost impossible with the inaccurate model and the FFT fringe search algorithm. Using multiple search windows to perform an extended FFT fringe search could be helpful, but the computation burden would be heavy and false detection would appear (see more details in Section 4). Other fringe fitting techniques (Schwab & William 1983; Alef & Porcas 1986) estimate the model residuals with VLBI data from multiple baselines. The VLBI fringe fitting with antenna based residuals (Alef & Porcas 1986) is used to improve the estimations of the FFT fringe search algorithm and its search range is not large either. Another technique named the global fringe search technique (Schwab & William 1983) requires good search initial values, which is also unavailable in the situations we concerned.

In this paper, a model-free fringe search with large search range and acceptable computation, called cross-ambiguity function (CAF) fringe search algorithm with wavelet boosting (CAF-W algorithm), is proposed for VLBI fringe search without priori predicted delay models. The CAFs make a coarse search in the delay–delay rate plane, and the estimations of the delay and delay rate are given by positioning the peak of the CAF amplitude. The wavelet boosting is used to eliminate the interference in the CAF amplitude and increase the output signal-to-noise rate (OSNR) of the CAF peak. The desired search range would be quite large so the sliding search window technique is used to cover the full range and control the computation burden. Both the CAF calculation and the wavelet boosting could be performed with fast algorithm for computation reduction. The estimated delay and delay rate are used to guide the FFT fringe search algorithm to get finer results. Then the correlation is able to be made successfully. The delay measurement results could be approximated to higher-order models so the correlation can be made again to get the delay measurements with higher precision.

The rest of the correspondence is organized as follows. In Section 2, we describe the basic theory of the VLBI correlation and the original VLBI correlation processing with priori predicted delay models. The CAF-W algorithm is proposed in Section 3. Section 4 shows the performance of our algorithm with VLBI observations results and compares the CAF-W algorithm with the extended FFT fringe search. Finally, conclusions are drawn in Section 5.

2. Theory of VLBI Correlation

In the basic VLBI correlation processing, the signals received and sampled at two telescopes could be denoted as

$$\begin{aligned} x_1(n) &= s_1(n) + w_1(n) \\ x_2(n) &= s_2(n) + w_2(n) \\ &= s_1[n + \tau(n)] + w_2(n), \end{aligned} \tag{1}$$

where $s_1(n)$ and $s_2(n)$ is the quasar signals sampled at two telescopes, $w_1(n)$ and $w_2(n)$ are the stationary, independent white noises. $s_2(n)$ is the delayed duplicate of $s_1(n)$ and $\tau(n)$ is the differential time delay, which represents the time difference between the two telescopes receive the same wavefront. $\tau(n)$ varies with time due to the relative motions between sources and telescopes. If the integration time is short enough that $\tau(n)$ could be treated as a constant, τ_0, $x_2(n)$ could be approximated as

$$x_2(n) = s_1(n + \tau_0) + w_2(n). \tag{2}$$

The constant time delay τ_0 could be got by the averaged cross-correlation of $x_1(n)$ and $x_2(n)$ as:

$$\begin{aligned} r_{12}(l) &= \frac{1}{MN} \sum_{m=0}^{M-1} \sum_{n=0}^{N-1-l} x_{1,m}(n + l) x_{2,m}^*(n) \\ &= \frac{1}{MN} \sum_{m=0}^{M-1} \sum_{n=0}^{N-1-l} x_1(n + l + mN) x_2^*(n + mN). \end{aligned} \tag{3}$$

N-point cross-correlation is averaged with M segments to decrease the estimation variance.

There are two methods to estimate τ_0 based on the cross-correlation function given in (3). The first method is called the time-domain method. In this method, $\tau_{12}(l)$ is calculated and the peak of its amplitude would be found at a certain position l_0 on the delay axis. Then the estimated time delay could be represented as $\hat{\tau}_0 = l_0 T_s$ where T_s is the sample period of $x_1(n)$ and $x_2(n)$.

Another method is called the frequency-domain method. The averaged cross-spectrum $S_{12}(k)$ could be calculated by discrete Fourier transform (DFT):

$$\begin{aligned} \mathrm{DFT}\{r_{12}\} = S_{12}(k) &= \frac{1}{M} \sum_{m=0}^{M-1} X_{1,m}(k) X_{2,m}^*(k) \\ &\approx e^{-j\frac{2\pi k \tau_0}{N}} |S_1(k)|^2. \end{aligned} \tag{4}$$

The cross-terms and the cross-spectrum of noises are ignored in (4) to simplify the discussion. $X_{1,m}(k)$, $X_{2,m}(k)$, and $S_1(k)$ are the DFT results of $x_{1,m}(n)$, $x_{2,m}(n)$, and $s_1(n)$. In VLBI observations of continuum emission sources, the amplitude of cross-spectrum is flat in the frequency domain. Its phase $\varphi_{12}(k) = -2\pi k \tau_0 / N$ is a straight line in the phase spectrum and τ_0 could be got by estimating its slope. The estimation accuracy is higher than the time-domain method, but its search range is limited by the group delay ambiguity problem. Since the phase can only be got between $\pm\pi$, the phase change between neighboring DFT frequency channels should be less than π. Therefore, the frequency-domain method provides high estimation accuracy with small measurement range.

The time delay $\tau(n)$ cannot be regarded as a constant when the integration time increases, so it is impossible to get the time delay estimation from (3) and (4) directly. The priori predicted delay model is needed to remove the time-varying terms before performing correlation. This procedure is called fringe rotation. Generally, the priori predicted delay models are approximated

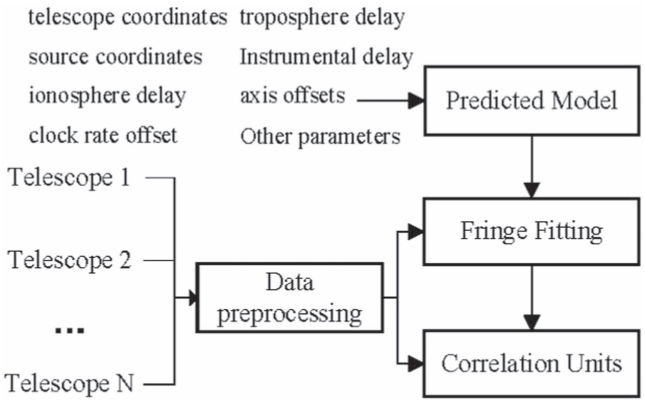

Figure 1. Block diagram of the original VLBI correlation.

to fifth order polynomial splines in the integration time:

$$\tau_m(t) = a_0 + a_1 t + a_2 t^2 + a_3 t^3 + a_4 t^4 + a_5 t^5 + o(t^5). \quad (5)$$

It is interpolated at sample period T_s and noted as $\tau_{\mathrm{m}}(n)$ below. Assume the telescope 1 is the reference telescope, the fringe rotation at telescope 2 for this baseline could be described as

$$\begin{aligned} x_2[n - \tau_m(n)] &= s_2[n - \tau_m(n)] + w_2[n - \tau_m(n)] \\ &= \mathrm{s}_1[n + \tau(n) - \tau_{\mathrm{m}}(n)] + w_2[n - \tau_m(n)] \\ &= \mathrm{s}_1[n + \Delta\tau(n)] + w_2[n - \tau_m(n)], \end{aligned} \quad (6)$$

where $\Delta\tau(n) = \tau(n) - \tau_m(n)$ is the residual of the time delay. It could be approximated as a small constant $\Delta\tau_0$ if the priori predicted delay model has enough precision, then the delay estimation is obtained by the frequency-domain method in VLBI.

The original VLBI correlation procedure is illustrated in Figure 1. The data provided by DBEs at telescopes are decoded and the raw data are fed to the fringe fitting module and correlation units. The residuals in the priori predicted delay models are estimated in the fringe fitting module then the revised delay models are used to perform correlation and make delay measurement.

3. CAF Fringe Search Algorithm with Wavelet Boosting

When the priori predicted delay models are not precise enough or even unavailable, it is hardly to make VLBI correlation or fringe fitting. Here we propose a CAF fringe search algorithm with wavelet boosting (CAF-W algorithm), which could be used to make successful correlation in these situations.

3.1. Averaged CAF Search

As we discussed in Section 2, the delay estimation could be made by calculating the cross-correlation. The problem is the long integration time required in VLBI observations would blur the correlation peak since the delay is time-variant (Johnson et al. 1983). In correlators, the fringe rotation is performed to "stop" the delay variation, which is implemented by multiplying the baseband signal with $\exp(-j2\pi f_{\mathrm{sky}}\dot{\tau}t)$. f_{sky} is the sky frequency of the signal received at antennas and $\dot{\tau}$ is the predicted delay rate got from the priori predicted delay model. A joint delay–delay rate estimation with large search range and enough precision would be able to make fringe search without priori predicted delay models.

The CAF is a classic time-frequency signal analysis technique for joint estimation of the differential time delay and Doppler frequency offset, which is widely used in radar, sonar, and acoustics signal processing (Boashash 2003). It could also be used in VLBI fringe search and the CAF for VLBI fringe search could be defined as

$$A_{12}(\dot{\tau}, \tau) = \int_0^T x_1(t) x_2^*(t - \tau) \exp(-j2\pi f_{\mathrm{sky}}\dot{\tau}t)dt, \quad (7)$$

where $\dot{\tau}$ is the trial delay rate and τ is the trial time delay. For continuum emission sources, the amplitude of the CAF would peak at the proper position in delay–delay rate plane.

The discrete L-point CAF for VLBI is expressed as

$$\begin{aligned} A_{12}(v, m) &= \sum_{n=0}^{L-m-1} x_1(n) x_2^*(n + m) \exp\left(-j2\pi \frac{v\Delta\dot{\tau}f_{\mathrm{sky}}n}{f_s}\right) \\ v &= -V/2, -V/2 + 1, \ldots V/2 \\ m &= -L/2 + 1, -L/2 + 2, \ldots L/2, \end{aligned} \quad (8)$$

where $\Delta\dot{\tau}$ is the search step of delay rate, f_s is the sample rate, m is the discrete lag on the delay axis, and V is the number of sampling points in the delay rate space. Similar to the cross-correlation function, the amplitude of the CAF would peak at the correct delay and delay rate in the delay–delay rate plane, so the estimations are given at discrete delay lags $\tau = mT_s$ and discrete delay rate $\dot{\tau} = v\Delta\dot{\tau}$.

The computation in (8) is $O(V \cdot (L^2 + L))$, which is evaluated by the times of complex multiplication. It would be too large to afford when L and V is large. A fast CAF algorithm with FFT is presented as Stein (1981):

$$A_{12}(v, m) = \sum_{k=0}^{L-1} X_1(k + v) X_2^*(k) \exp\left(-j2\pi \frac{mk}{L}\right). \quad (9)$$

The notation $X_1(k)$ and $X_2(k)$ refer to the L-point FFT of $x_1(n)$ and $x_2(n)$, and the computation could be reduced to $O((V + 2) \cdot L \log_2 L)$. Although the cyclical convolution is widely used in VLBI correlators, it would cause estimation errors in the CAF search. To perform the linear convolution, the FFT size L must be at least twice as the length of the valid samples in $x_1(n)$ and $x_2(n)$.

Since the delay rate compensation in (9) is performed by shifting the discrete frequency channels of FFT, the loss of the

CAF's amplitude peak is unavoidable due to the delay rate mismatch. The delay rate mismatch $e(\dot{\tau})$ satisfies

$$|e(\dot{\tau})| \leqslant 0.5\Delta\dot{\tau} = 0.5\frac{1}{f_{\rm sky}}\frac{f_s}{L}. \tag{10}$$

The amplitude degradation factor D satisfies

$$D = \frac{\sin(\pi f_{\rm sky} T_c\ |e(\dot{\tau})|/2)}{\pi f_{\rm sky} T_c\ |e(\dot{\tau})|/2} \leqslant \frac{\sin(0.25\pi)}{0.25\pi} \approx 0.9 \approx -0.91\ \text{dB} \tag{11}$$

where $T_c = L/f_s$ is the correlation time of the CAF processing. In the worst case, the maximum peak loss is less than 1 dB, which is acceptable in practice (Adams et al. 1980).

The search range of the L-point CAF is calculated as follows. According to the discussion in Patzewitsch et al. (1978), the -3 dB point of the CAF amplitude on the delay axis could be calculated as

$$1 - \frac{|\tau|}{T_c} \geqslant 0.707, \qquad |\tau| < 0.3T_c. \tag{12}$$

The -3 dB τ-width is $0.3T_c$ so the reliable search range in the delay direction is $0.3L/f_s$. And the search range on the delay rate space is $V\Delta\dot{\tau}$. The maximum geometric delay rate that can be encountered on terrestrial baselines in quasar observations satisfies $|\dot{\tau}_{\rm max}| \leqslant 1.5\ \mu\text{s s}^{-1}$ (Keimpema et al. 2015), so V could be calculated by f_s and $f_{\rm sky}$ as

$$V \geqslant \frac{2\ |\dot{\tau}_{\rm max}|\ f_{\rm sky}}{f_s} L. \tag{13}$$

Increasing the correlation time T_c could increase the peak's OSNR and the search range in the delay direction, but it is limited by the permissible FFT length and would increase the computation burden rapidly. Incoherent averaging technique offers an effective trade-off between the computation burden and the peak's OSNR loss (Scarbrough et al. 1983). A data window with N samples is divided into R overlapped (or not) segments with $L/2$ samples, and L-point CAF is calculated with each corresponding pair of segments, then the amplitudes are averaged, as it illustrates in Figure 2. Comparing with calculating $2N$-point CAF directly, the computation burden could be reduced from $(V+2)2N\log_2(2N)$ to $R(V+2)L\log_2 L$.

3.2. Wavelet Boosting

The peak detection should be done in the CAF search plane to get the estimated delay and delay rate. However, it is difficult since the averaged CAF amplitude has a strong window-effect interference in the delay direction, as shown in Figure 3. According to (9), the CAF amplitude should have a sinc-like behavior in the delay rate space as well. The response in rate space in Figure 3 seems to be very flat because the number of the sampling points in rate space (V) is far less than the FFT length (L). The data used in Figure 3 is observed at 8470 MHz and sampled at 8 MS s^{-1}. L is chosen to be 8192 so V is 26 based on (13).

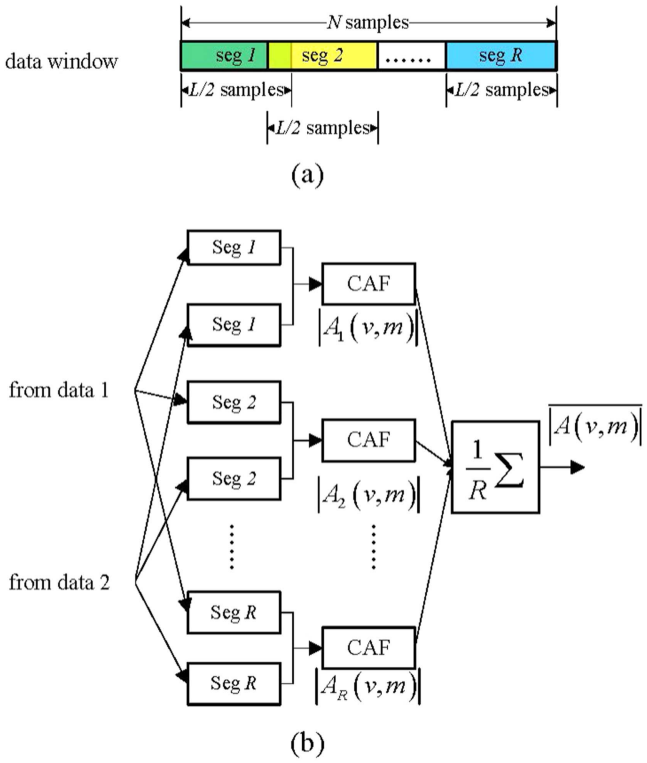

Figure 2. Illustration of the incoherent averaging technique.
(A color version of this figure is available in the online journal.)

Noted that the interference in the delay space is a slow varying component in the delay direction, while the CAF peak is a pulse-like term. Therefore, a high-pass filter in the Fourier transform domain of delay seems to be able to remove the interference. However, high-pass filters would also broaden the CAF peak and decrease the OSNR of the CAF peak. Here, the wavelet boosting is proposed to get rid of the interference in the averaged CAF amplitude.

The wavelet boosting is based on the wavelet multiresolution analysis (MRA) (Donoho 1993) and is inspired by the wavelet de-noising method (Vetterli & Herley 1992; Rosas-Orea et al. 2005). Assume the signal $f(x)$ has a finite energy, then the discrete orthogonal wavelet decomposition at resolution level j is calculated as (Mallat 1989)

$$a_j(k) = \int f(x)\phi(2^{-j}x - k)dx, \tag{14}$$

$$d_j(k) = \int f(x)\psi(2^{-j}x - k)dx \tag{15}$$

where $\phi(x)$ is scaling function, $\psi(x)$ is wavelet function, $a_j(k)$ are approximate coefficients and $d_j(k)$ are detail coefficients. Both j and k should be integer. $\phi(x)$ and $\psi(x)$ are used as pairs. The approximate function $f_j(x)$ and the detail function $g_j(x)$ at

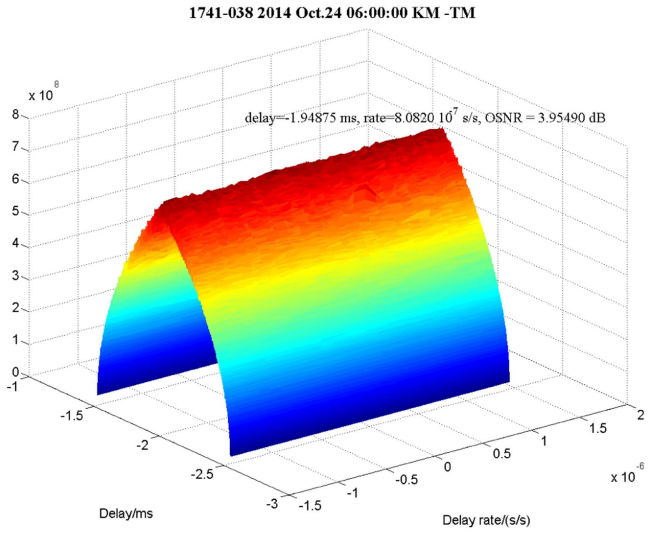

Figure 3. Averaged CAF amplitude in the delay–delay rate plane contained the CAF peak.
(A color version of this figure is available in the online journal.)

level j are got as

$$f_j(x) = \sum_k a_j(k)\phi(2^{-j}x - k), \tag{16}$$

$$g_j(x) = \sum_k d_j(k)\psi(2^{-j}x - k). \tag{17}$$

For a total J level decomposition, the original function $f(x)$ could be reconstructed perfectly as

$$f(x) = f_J(x) + \sum_{j=1}^{J} g_j(x). \tag{18}$$

The orthogonal wavelet MRA is commonly performed by cascaded Finite Impulse Response (FIR) filter banks (Mallat 1989). Figure 4 illustrates how the wavelet decomposition is implemented and how to get the detail and approximate functions by the cascaded filter banks. The detail coefficients $d_j(k)$ and the approximate coefficients $a_j(k)$ at each level are got by the decomposition filters ($\widetilde{G}$ and $\widetilde{H}$) and decimators. Then the detail and approximate function at resolution level j are reconstructed by reconstruction filters G and H, respectively. $\widetilde{X}$ indicates the mirror filter (or called symmetric filter) of X, whose impulse response is defined as $\tilde{x}(n) = x(-n)$. The filter coefficients are determined once the wavelet function is selected.

The principle of the wavelet boosting is to separate the CAF peak and the interference with MRA. The scaling filters H are low-pass filters and the wavelet filters G are high-pass filters. Unlike the classic high-pass filter in the Fourier transform domain, the wavelet filter (high-pass) is performed on different resolution levels. Therefore, the high frequency components

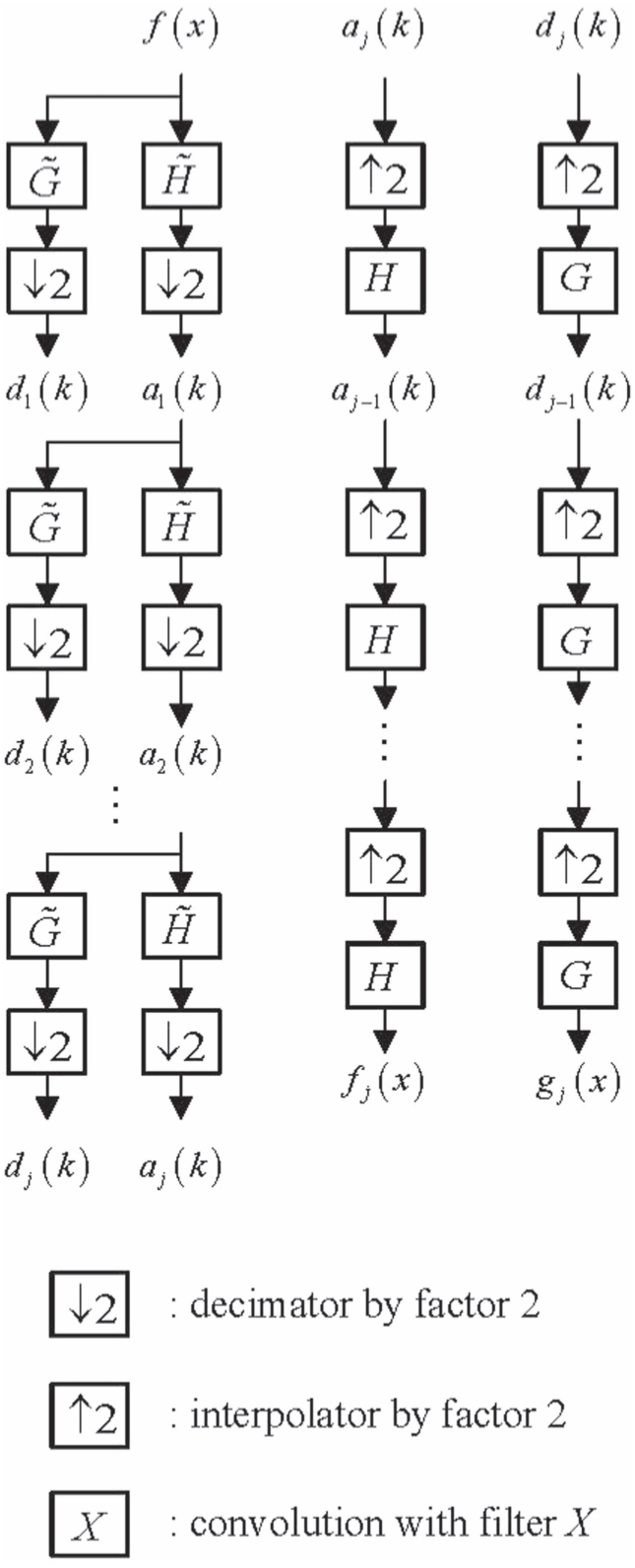

Figure 4. Wavelet MRA implemented by filter banks.

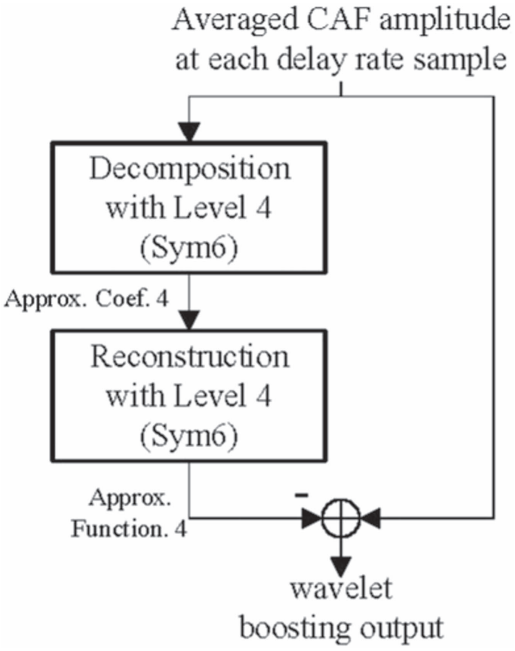

Figure 5. Diagram of the wavelet boosting.

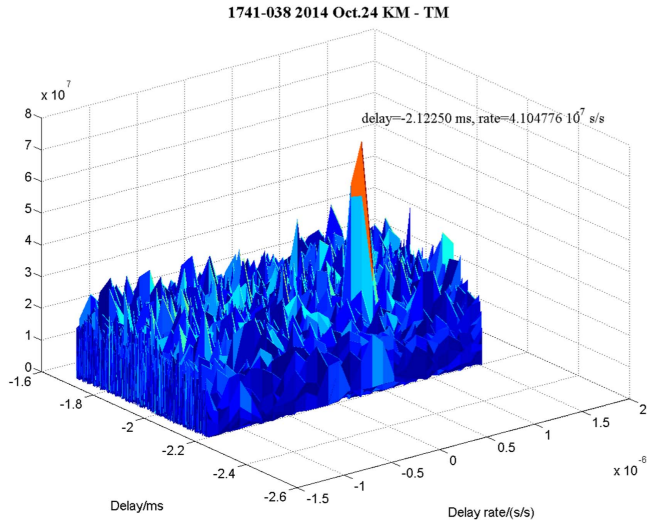

Figure 6. In the CAF-W search plane, the CAF peak appears after the window-like interference is removed.
(A color version of this figure is available in the online journal.)

could be achieved without broadening features. The detail functions only contain the peak-like components and the approximate function at coarse resolution level retains the window-like interference. Although the CAF peak is only included by the detail functions, they cannot be used as the output of the wavelet boosting because it is difficult to determine how many resolution levels contain the CAF peak and an inappropriate choice would decrease the OSNR of the CAF peak. Alternatively, the approximate function is removed from the original averaged CAF amplitude so the filtered amplitude is achieved.

Selecting an appropriate wavelet function and resolution level are important. After several trials, the Symlet wavelets with order six (noted as Sym6) is selected and the resolution level is set to be four, which has the best OSNR boosting performance. The Symlet wavelets are orthogonal and biorthogonal wavelets with least asymmetry, which is proposed by Daubechies from the famous Daubechies wavelet (Daubechies 1992). The scaling and wavelet filters of Sym6 are both 12th-order FIR filters and their coefficients are given in Daubechies (1992).

The procedure of the wavelet boosting is summarized as follows. The averaged CAF amplitude is sliced along the delay axis at each sample of delay rate. These amplitude-delay functions are decomposed to resolution level four by filter banks. Only the approximate function on level four is reconstructed from the approximate coefficients and removed by subtraction. Figure 5 illustrates a simple diagram of the wavelet boosting. Figure 6 shows the same search plane in Figure 3 after wavelet boosting and the CAF peak is strong enough for peak detection.

3.3. Large Range Delay Search Based on Sliding Window

According to (12), the delay search range of the CAF-W algorithm is less than $0.3T_c$, which is limited by the FFT length and the computation requirement. However, in a real observation the delay search range would be quite large when the priori predicted delay models are unavailable.

A sliding window is used to cover the large search range in the delay space without increasing the correlation time and take control of the computation burden. The CAF-W algorithm is performed with raw data from two telescopes, and the data window of data 2 is shifted with M samples in the time space. Since the data window of data 1 is fixed, the center of the search window moves MT_s on the delay axis, as it shows in Figure 7. The shift in the delay space cannot be larger than $0.3T_c$ so M is chosen to be $0.25L$. Here we just discuss the search window along the delay axis though it is actually a 2D plane.

3.4. Overall CAF-W Algorithm

Figure 8 illustrates the overall CAF-W algorithm in the VLBI observations. The priori predicted delay models are replaced by the CAF-W algorithm. The averaged CAF search is performed with the raw VLBI data from each baseline and the

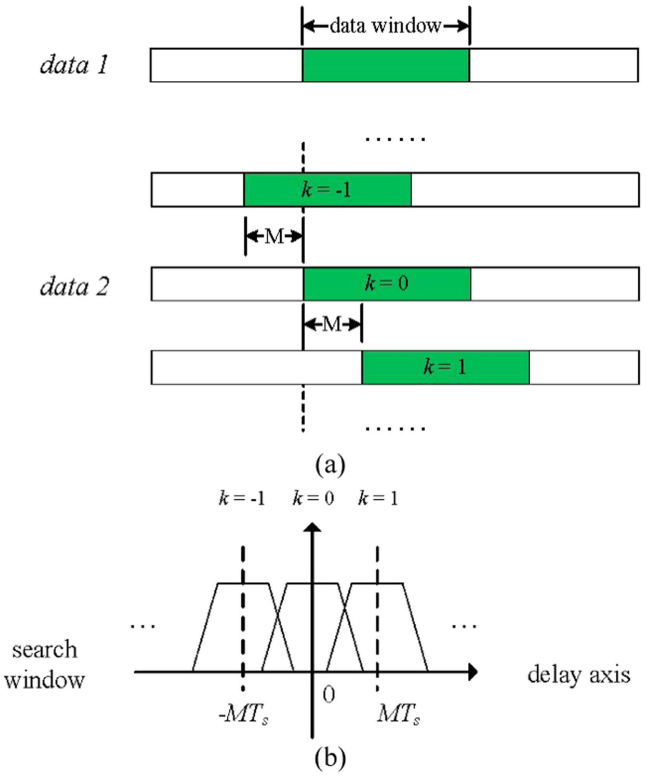

Figure 7. Data window (in green) only moves on data 2, so the search window would slide on the delay axis.
(A color version of this figure is available in the online journal.)

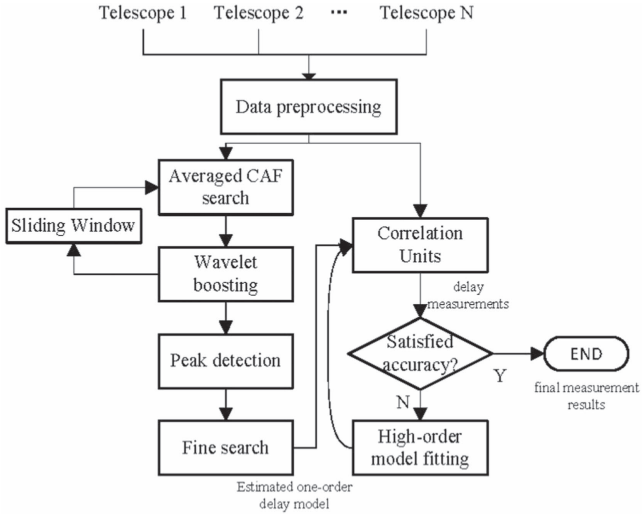

Figure 8. Diagram of the VLBI correlation procedure using CAF-W algorithm.

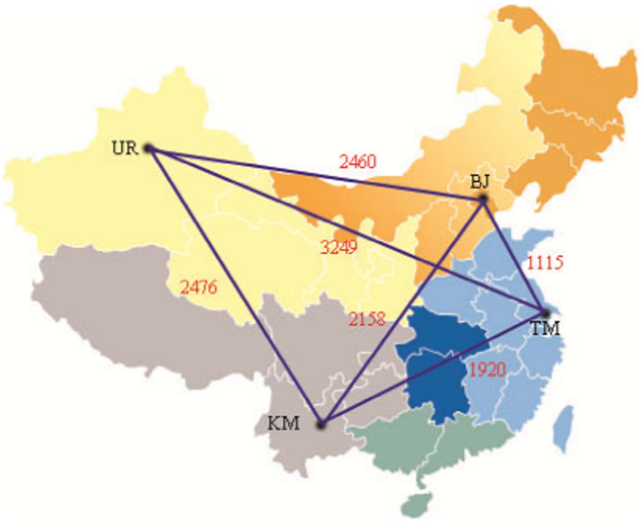

Figure 9. Geographical distribution of CVN. The numbers in red are the length of baselines in kilometers.
(A color version of this figure is available in the online journal.)

wavelet boosting is performed before peak detection to increase the CAF peak's OSNR. Then the data window slides along the delay space until the CAF peak is found. The coarse delay and delay rate estimations guide the fine search module (e.g., FFT fringe search algorithm) to give a finer one-order delay model and the group delay measurements are made. After a series of the group delay measurements have been got, a high-order delay model with higher accuracy, called the post-correlation delay model, could be got by polynomial fitting of these group delay measurements results, and then the group delay could be got with better accuracy.

4. Experiment Results

4.1. Search Results of CAF-W Algorithm

The CAF-W algorithm has been verified by the VLBI observation data. An observation of source 1741-038 was performed at X band by the Chinese VLBI network (CVN). Figure 9 shows the telescopes and baseline lengths of CVN (Li et al. 2007; Huang et al. 2014). In this observation, a new kind of DBE was deployed at Station Tianma (TM) and its data is used to make correlation with the data recorded by routine DBEs at Station Kunming (KM) and Urumqi (UR). All DBEs sample and record raw data with 4 MHz bandwidth in either real or complex data type.

At first, a priori predicted delay model for the routine DBEs was provided to make correlation on KM-TM baseline between the new DBE and the routine DBE. The phases of the cross-spectrum plotted in Figure 10(a) show no sign of interference fringe. Considering the provided priori predicted delay model was not appropriate to the new DBE, the FFT fringe search

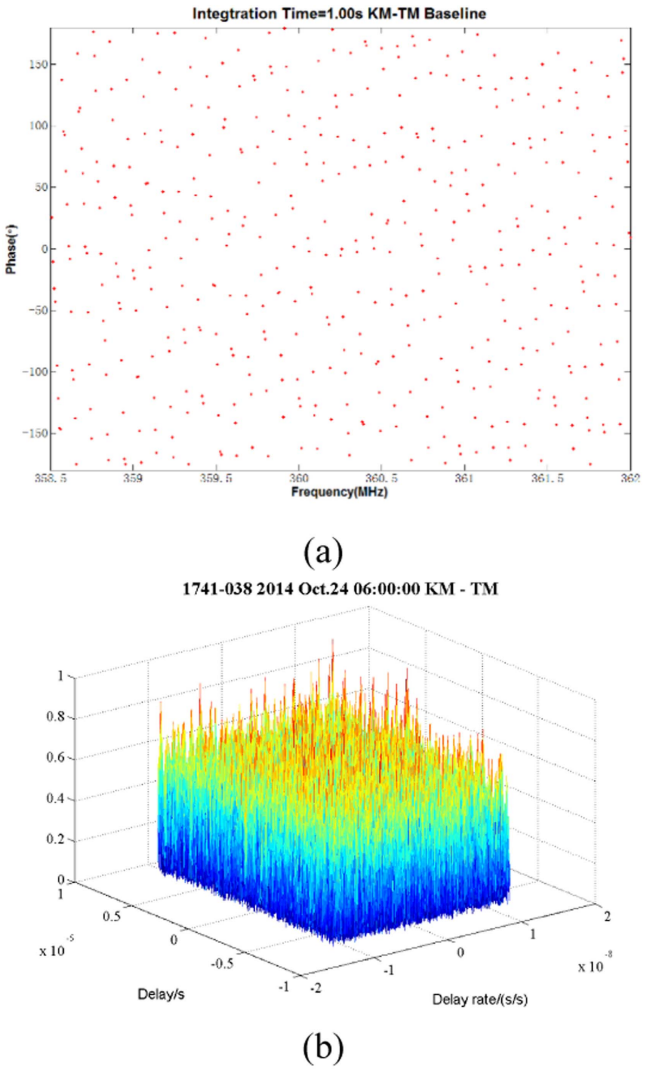

Figure 10. (a) phases of cross-spectrum and (b) the search plane of the FFT fringe search algorithm.
(A color version of this figure is available in the online journal.)

algorithm was performed and the delay–delay rate plane is showed in Figure 10(b). However, no peak appears in the search plane.

Then, by not using this priori predicted delay model, the CAF-W algorithm is used to find the fringe from the raw data. The data window length is set to be about 1 s and the segments number of the incoherent averaging (R) is 250. According to the length of the KM-TM baseline, the search range of delay is set to be 12 ms. The CAF-W search plane with the CAF peak is showed in Figure 11(a). Figure 11(b) gives the OSNR of the maximum peak in each search window and shows that the CAF peak is about 10 dB higher than others. The estimated delay and delay rate are used to perform the fine search by FFT fringe

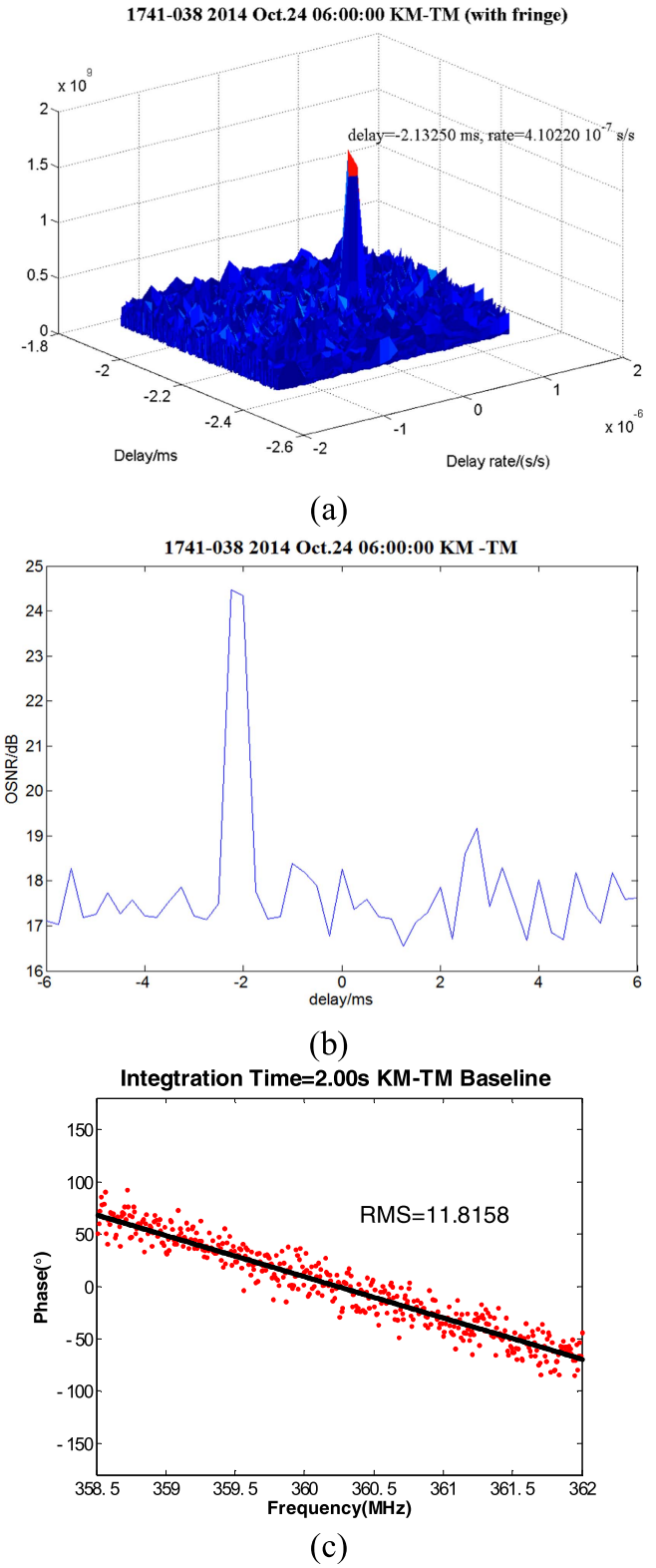

Figure 11. (a) CAF-W search plane with the CAF peak; (b) OSNR of peak in each search window; and (c) the fringe phases got with the estimated delay model.
(A color version of this figure is available in the online journal.)

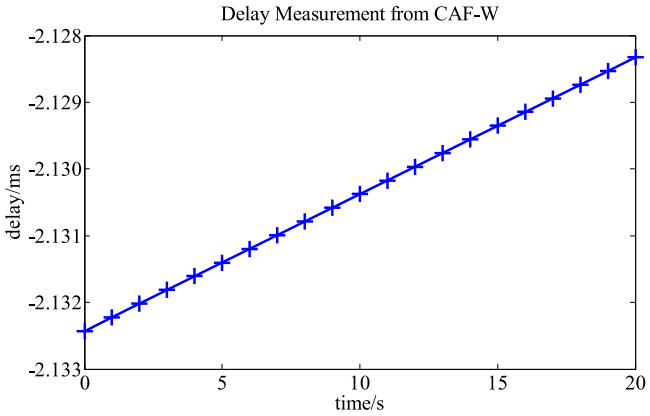

Figure 12. Delay measurement results with the estimated one-order model. (A color version of this figure is available in the online journal.)

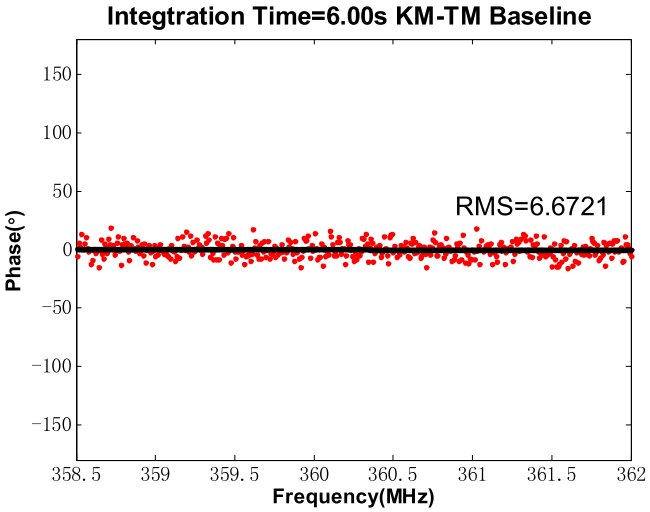

Figure 13. Fringe phases using the post-correlation delay model. (A color version of this figure is available in the online journal.)

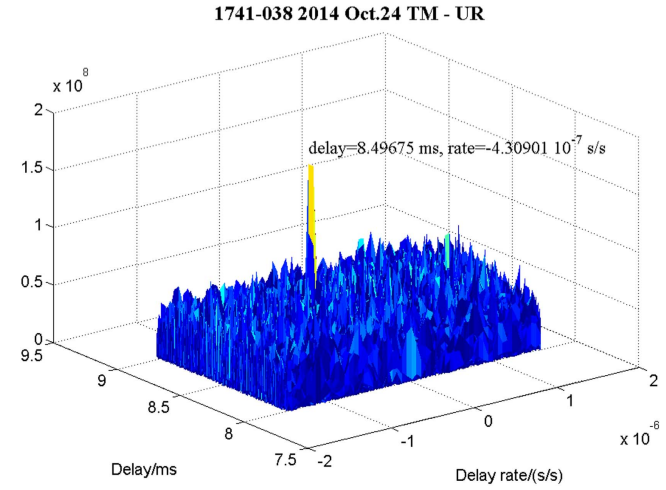

Figure 14. CAF-W search plane of TM-UR baseline with the CAF peak. (A color version of this figure is available in the online journal.)

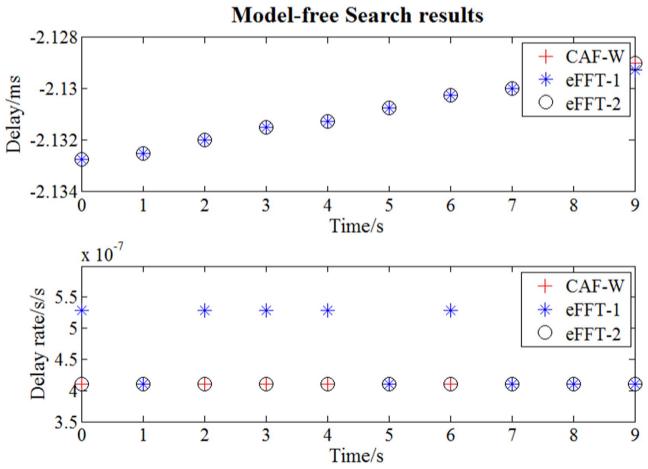

Figure 15. Search results with different methods and grid parameters. (A color version of this figure is available in the online journal.)

Table 1
Parameters of Model-free Fringe Searches

Name of method	CAF-W	eFFT-1	eFFT-2
Number of windows on delay space	51	26	26
Search range of each window on delay space (ms)	±0.512	±0.512	±0.512
Shift of each window on delay space (ms)	0.256	0.512	0.512
Delay resolution in each window (μs)	0.125	0.125	0.125
Number of windows on delay rate space	1	26	51
Search range of each window on delay rate space (s s^{-1})	±1.5e-6	±5.91e-8	±5.910e-8
Shift of each window on delay rate space (s s^{-1})	/	1.182e-7	5.910e-8
Delay rate resolution in each window (s s^{-1})	1.157e-7	1.44e-11	1.44e-11
Number of segment in averaging	250	125	125
Average elapsed Time (s)	50.3	6984.8	14648.8

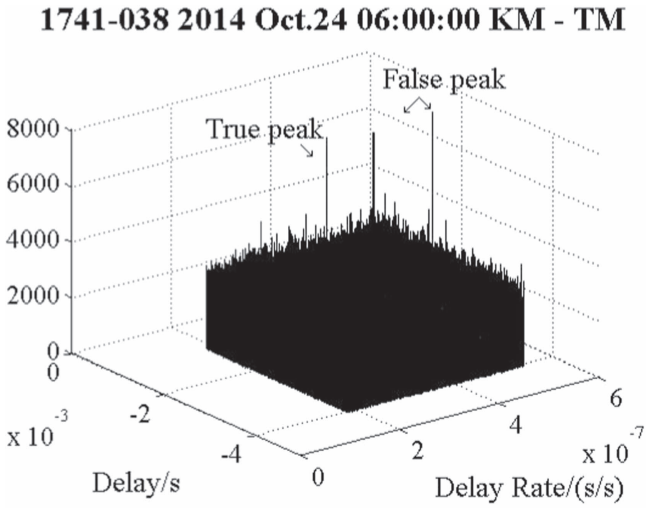

Figure 16. Search windows of eFFT-1 fringe search with true and false peaks.

search. Then the correlation processing is made successfully and the fringe phases are showed in Figure 11(c).

The CAF-W algorithm is performed on the entire provided VLBI data and the correlation is made with the estimated one-order delay model at each second. The delay results are showed in Figure 12. Then the post-correlation delay model mentioned in Figure 8 is got by a 5th order polynomial fitting. It is a more precise delay model, which is able to replace the priori predicted delay model. The correlation using the post-correlation delay model could be made with a longer integration time and the fringe phases are showed in Figure 13. The fringe is clearer and the root mean square (rms) of the linear fitting are less than that in Figure 11(c).

The difference between the post-correlation delay model and the provided priori predicted delay model is about 10 μs. We infer this offset is mainly caused by the differences in the signal propagation paths and instrument delays between two kinds of DBEs since it is the first observation with the new DBE.

CAF-W algorithm also give the estimated delay model of a longer baseline (TM-UR) successfully, and Figure 14 shows the CAF-W search plane with the CAF peak.

4.2. Comparison with FFT Fringe Search

As comparison, an extended FFT fringe search is performed in the same situation. Because the search window of original FFT fringe search is narrow on both delay and delay rate space, the entire delay and delay search range has to be divided into multiple search windows. The largest peak among all these windows is treated as the fringe peak and its position would give the delay and delay rate estimations. This method is called eFFT fringe search (extended FFT fringe search) in this paper.

Two eFFT fringe search algorithms with different window size are used and named eFFT-1 and eFFT-2, respectively, in this paper. The detailed parameters of these searches are indicated in Table 1. The delay and delay rate estimation results given by CAF-W algorithm, eFFT-1 and eFFT-2 are illustrated in Figure 15. The delay rate curve of eFFT-1 shows obvious outliers at several points, which are caused by false detection. In order to find the reason of the false detection in eFFT-1, Figure 16 shows the search windows of three adjacent grid nodes. Obviously there are two strong peak at different position, and the false peak is larger than the true peak, which causes false detection. In contrast, there is no false detection problem in CAF-W algorithm.

The problem of false detection in eFFT-1 could be solved by decrease the shift of each window on the delay rate space. In eFFT-2, it is decreased by half and the false detection no longer happened. However, the computation time increases rapidly. The average computation elapsed times of CAF-W, eFFT-1 and eFFT-2 are also given in the last line of Table 1. The computation of eFFT-1 is 139 times of that of CAF-W and it has trouble with false detection, while the eFFT-2 gives a successful search result but its computation is 291 times as CAF-W algorithm. The speed-up factor of CAF-W is that its search window only shift on the delay space while the eFFT have to slide on both delay and delay rate space, so there are less search windows in CAF-W algorithm.

5. Conclusions

This paper presents a model-free CAF fringe search algorithm with wavelet boosting for VLBI observation. It is able to estimate a coarse one-order delay model for the fringe fitting even if the priori predicted delay models are unavailable. Incoherent averaging CAF performs the joint delay–delay rate estimation and the wavelet boosting is used to remove the serious interference in the search plane. The large search range in the delay direction is implemented by the sliding search window technique to reduce computation burden. The CAF and wavelet boosting calculation could be accelerated by fast algorithms. The CAF-W algorithm is verified with the raw data from VLBI quasar observations and VLBI correlation is made successfully. The extended FFT fringe search is performed to make model-free fringe search as a comparison and its computation of CAF-W is far more than that of CAF-W algorithm.

We gratefully acknowledge support of the National Natural Science Foundation of China (U1531104, 11373061, 11573057) and the Program of Shanghai Subject Chief Scientist (14XD1404300). The authors gratefully acknowledge the referees for helpful comments and suggestions.

References

Adams, W. B., Kuhn, J. P., & Whyland, P. W. 1980, ITASS, 28, 158
Alef, W., & Porcas, R. W. 1986, A&A, 168, 365
Boashash, B. 2003, Time-frequency Signal Analysis and Processing: A Comprehensive Reference (Amsterdam: Elsevier)
Clark, T. A., Corey, A. E., Davis, J. L., et al. 1985, ITGRS, 4, 438

Cotton, W. D. 1995, in ASP Conf. Ser. 22, Very Long Baseline Interferometry and the VLBANRAO, Vol. 82 (San Francisco, CA: ASP), 189
Counselman, C. C., III 1973, IEEEP, 61, 1225
Daubechies, I. 1992, in Ten Lectures on Wavelets (Philadelphia, PA: SIAM)
Donoho, D. L. 1993, in Proc. Symp. in Applied Mathematics (Washington, DC: American Mathematical Society), 173
Huang, Y., Chang, S., Li, P., et al. 2014, ChSBu, 59, 3858
Johnson, G. W., Ohlms, D., & Hampton, M. 1983, in Int. Conf. on ICASSP'83, Vol. 8, Acoustics, Speech, and Signal Processing (New York: IEEE), 583
Keimpema, A., Kettenis, M. M., Pogrebenko, S. V., et al. 2015, ExA, 39, 259
Li, J. L., Guo, L., & Zhang, B. 2007, in Proc. IAU Symp. 248., A Giant Step: from Milli- to Micro-arcsecond Astrometry, Vol. 3 (Cambridge: Cambridge Univ. Press), 182
Mallat, S. G. 1989, ITPAM, 11, 674
Marcello, F., & Spencer, R. E. (ed.) 1989, Very Long Baseline Interferometry: Techniques and Applications, Vol. 283 (Dordrecht: Kluwer Academic Publishers), https://doi.org/10.1007/978-94-009-2428-4
Moran, J. M. 1976, MExP, 12, 228
Nakajima, J., Koyama, Y., Sekido, M., et al. 2001, ExA, 11, 57
Patzewitsch, J. T., Srinath, M. D., & Black, C. I. 1978, ASAJ, 64, 1412
Petrov, L., Hirota, T., Honma, M., et al. 2007, AJ, 133, 2487
Romney, J. D. 1995, in ASP Conf. Ser. 22, Very Long Baseline Interferometry and the VLBANRAO, Vol. 82 (San Francisco, CA: ASP), 17
Rosas-Orea, M. C. E., Hernandez-Diaz, M., Alarcon-Aquino, V., & Guerrero-Ojeda, L. G. 2005, in 5th Int. Conf. on Electronics, Communications and Computers (New York: IEEE), 125
Scarbrough, K., Tremblay, R. J., & Carter, G. C. 1983, ITASS, 31, 1191
Schwab, F. R., & William, D. C. 1983, AJ, 88, 688
Stein, S. 1981, ITASS, 29, 588
Vetterli, M., & Herley, C. 1992, ITSP, 40, 2207